First-principles determination of charge carrier mobility in disordered semiconducting polymers

Xu Zhang, Zi Li, and Gang Lu
Department of Physics and Astronomy, California State University–Northridge, Northridge, California 91330-8268, USA
(Received 5 August 2010; revised manuscript received 6 October 2010; published 19 November 2010)

We propose a theoretical method that can predict carrier mobility in disordered semiconducting polymers and organic semiconductors from first principles. The method is based on nonadiabatic *ab initio* molecular dynamics and static master equation, treating dynamic and static disorder on the same footing. We have applied the method to calculate the hole mobility in disordered poly(3-hexylthiophene) conjugated polymers as a function of temperature and electric field and obtained excellent agreements with corresponding experimental results. The method could be used to explore structure-mobility relation in disordered semiconducting polymers/organic semiconductors and aid rational design of these materials.

DOI: 10.1103/PhysRevB.82.205210 PACS number(s): 72.20.Ee, 71.15.Pd, 72.80.Le

Disordered semiconducting polymers and organic semiconductors have received significant attention recently for their potential applications in light-emitting diodes,[1] field-effect transistors,[2] photovoltaics,[3] etc. The disordered nature of these organic materials render them more flexible, lighter, and more cost effective to process than their inorganic counterparts. However, one of the major bottlenecks that limits the efficiency of the disordered semiconductor devices is their poor charge carrier mobility. Therefore it is of great scientific and technological importance to understand underlying physical processes and, in particular, to develop theoretical tools that can predict the carrier mobility from first principles.

The charge transport in the disordered conjugated polymers and organic semiconductors have been studied extensively in the past decades and two popular classes of models have emerged in literature: polaron models and disorder models.[4] In the polaron models, the charge transport is characterized by the dynamic disorder arising from electron-phonon coupling. Model Hamiltonians such as Holstein and Peierls types have been widely used with mixed success.[5–7] Often based on perturbation theories, these models are limited in scope with restrictions to specific ranges of microscopic parameters and temperatures.[4] On the other hand, the static disorder models which capture structural randomness, including Miller-Abrahams[8] and Marcus[9] theories, have been proposed to calculate the hopping rates between sites.[10–15] The widely used Gaussian mobility model belongs to this category.[10,11] The major weakness of the disorder models is that they are not material specific and in general contain empirical parameters. Therefore a successful theory of the charge transport should include ingredients of both models and describe the dynamic and static disorders in a realistic manner. Toward this goal, significant advances have been made recently, including the Marcus theory with *ab initio* determined microscopic parameters,[16–20] the construction of model Hamiltonians with the transfer integrals evaluated quantum mechanically,[21–23] and using time-dependent perturbation theory to determine the phonon-assisted transition rate,[24,25] among others. However, all these methods have certain elements of empiricism, relying on classical force fields to compute material structure and/or phonon spectrum. In addition, many of these methods are based on the perturbation theories and/or the harmonic approximation of phonons, which may not always be valid.

In this paper, we propose an *ab initio* approach that can predict charge carrier mobility in disordered conjugated polymers and organic semiconductors as a function of temperature, electric field, and carrier concentration, *entirely* from first principles; i.e., there is no empirical input or adjustable parameter in the simulations. This approach is based on the *ab initio* nonadiabatic molecular dynamics (MD) (Refs. 26 and 27) for simulating phonon-assisted electron transitions between localized electronic states in disordered systems. The electronic energy levels and their transition rates are determined from the density-functional theory, taking into account of both intermolecule and intramolecule (or chain) contributions. Treating both the dynamic disorder and the static disorder at an equal footing, the approach is quite general and does not involve the perturbation theories or the harmonic approximation of phonons. In conjunction with the macroscopic master equation, this approach allows us to study the electron transport in length scales that are relevant to realistic devices. As an example, we have applied this approach to determine the hole mobility in poly(3-hexylthiophene) (P3HT) polymers at various temperatures and electric fields and obtained excellent agreements with experiments. It is expected that the approach could be used to elucidate the structure-mobility relations and aid rational design of these materials.

In disordered semiconductors, the electronic states are spatially localized and the electron transport could be regarded as random walks in the real and the energy space.[10] The thermal fluctuations of the ions lead to overlaps between the localized electronic states in space and energy, thus promote electronic transitions between the states as depicted schematically in Fig. 1(a). A charge carrier (electron or hole) initially resides in the red state; as the red and blue states evolve under the influence of phonons, at some point the red state starts overlapping with the blue one, and as a result, the charge carrier transfers to the unoccupied blue state. Therefore our first goal is to determine this probability or the transition rate.

The time-dependent one-electron wave function of the carrier (electron or hole) is $\psi(\mathbf{r},t)$ which is expanded in the adiabatic Kohn-Sham (KS) orbitals $\phi_i[\mathbf{r},\mathbf{R}(t)]$

 ©2010 The American Physical Society

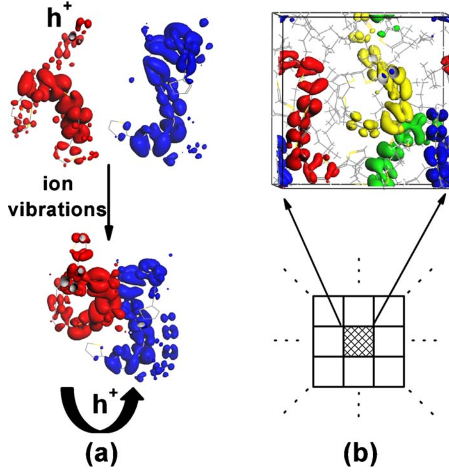

FIG. 1. (Color online) Schematic representation of the model. (a) Hopping of a hole (h^+) assisted by phonons. Red and blue colors denote the localized electronic states in two separated P3HT chains, where the red state is occupied by the hole. Thermal vibrations of the ions lead to overlap between the two states promoting the hole transition from the red state to the blue state. (b) The system is divided into $l_x \times l_y \times l_z$ boxes; each box has a dimension of a few nanometers (in this particular case, the dimension of the box is 1.8 nm). Atomic structure and isosurfaces of several valence bands are shown in the representative box. The top four valence bands are shown in red, blue, yellow, and green, respectively. The electronic states are spatially localized over a length scale of a few angstroms.

$$\psi(\mathbf{r},t) = \sum_j c_j(t)\phi_j[\mathbf{r},\mathbf{R}(t)], \tag{1}$$

where $c_j(t)$ is the expansion coefficient and $\phi_i[\mathbf{r},\mathbf{R}(t)]$ is the eigenstate of the KS Hamiltonian for the current ionic positions $R(t)$. Let the carrier start in the KS state i at $t=0$, i.e., $\psi(\mathbf{r},0)=\phi_i[\mathbf{r},\mathbf{R}(0)]$, the evolution of the coefficient $c_j^{(i)}(t)$ is given by[26,27]

$$\frac{\partial}{\partial t}c_j^{(i)}(t) = -\sum_k c_k^{(i)}(t)\left(\frac{i}{\hbar}\epsilon_k\delta_{jk} + d_{jk}\right), \tag{2}$$

where ϵ_k is the energy of the kth KS orbital and d_{jk} is the nonadiabatic coupling between the jth and kth KS orbitals

$$d_{jk} \equiv \langle\phi_j|\nabla_{\mathbf{R}}|\phi_k\rangle\cdot\frac{d\mathbf{R}}{dt} = \langle\phi_j|\frac{\partial}{\partial t}|\phi_k\rangle. \tag{3}$$

Therefore $|c_j^{(i)}(t)|^2$ represents the transition probability that the carrier is hopping from the state i to the state j during the time interval δt (in this case $\delta t=t-0$). As the result, the transition rate from the state i to j is given by $\langle|c_j^{(i)}(t)|^2/t\rangle$, averaging over the molecular-dynamic trajectory during δt. To ensure the detailed balance, the thermal equilibrium microscopic transition rate $\gamma_{i,j}$ is defined as[28]

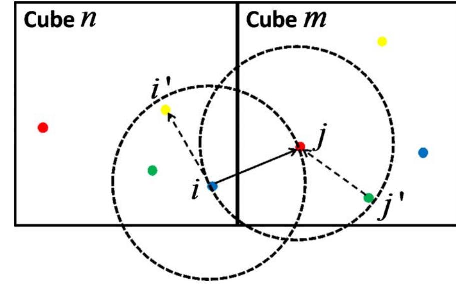

FIG. 2. (Color online) Schematic spatial position of the localized states in two neighboring cubes n and m. The red, blue, yellow, and green points in cube n correspond to the spatial position of the localized electronic states shown in Fig. 1(b).

$$\gamma_{i,j} = \begin{cases} \left\langle \dfrac{|c_j^{(i)}(t)|^2}{t} \right\rangle \exp\left(-\dfrac{\epsilon_j-\epsilon_i}{k_B T}\right) & \text{if } \epsilon_j \geq \epsilon_i, \\ \left\langle \dfrac{|c_j^{(i)}(t)|^2}{t} \right\rangle & \text{if } \epsilon_j < \epsilon_i. \end{cases} \tag{4}$$

Next we switch to the macroscopic scale (100 nm and beyond) for which the carrier mobility is calculated. Specifically, the material is divided into $l_x \times l_y \times l_z$ boxes as shown in Fig. 1(b). Each box should be chosen as large as computationally feasible but the minimal dimensions of the box should be greater than the intersite distance used in the Gaussian mobility models.[10] To simulate the static disorder, each box is randomly chosen and randomly rotated from the snapshots of the molecular-dynamics trajectory. To assist the evaluation of the microscopic transition rate across neighboring boxes, we associate each localized state with a position vector in the real space. First, we calculate the average position of the localized state i by the first moment of its charge density via $\bar{\mathbf{r}}=\int\rho_i(\mathbf{r})\mathbf{r}d\mathbf{r}$, where $\rho_i(\mathbf{r})=|\phi_i(\mathbf{r})|^2$ is the charge density of the state i. Second, we determine the root-mean-square deviation of the average position by $\delta\mathbf{r} = \sqrt{\int\rho_i(\mathbf{r})(\mathbf{r}-\bar{\mathbf{r}})^2 d\mathbf{r}}$. Finally, the spatial position of the localized state can be obtained by a random selection from the range $[\bar{\mathbf{r}}-\delta\mathbf{r},\bar{\mathbf{r}}+\delta\mathbf{r}]$. The above procedure applies to all boxes, with the localized wave functions in different boxes correspond to different (but random) snapshots of the wave functions from *ab initio* MD trajectory; the wave functions are also rotated randomly before placed in each box. In Fig. 2, we show schematically the positions of the top four valence bands plotted in Fig. 1(b). As discussed later, the microscopic transition rate across the neighboring boxes is calculated based on these positions and an average has to be taken over the random selections. On the other hand, the intrabox transition rate is determined by Eq. (4) and does not depend on the position vectors.

The macroscopic transition rate of the charge carrier from box n to box m, $\Gamma_{n\to m}$ is given by summing up the microscopic transition rates,

$$\Gamma_{n\to m} = \sum_{i\in n} p_n f_i \sum_{j\in m} \gamma_{i,j}(1-p_m f_j), \tag{5}$$

where the summations of i and j are over all relevant electronic states of the carrier in box n and m, respectively. For

the electron (hole) carrier, the relevant states are from the conduction (valence) bands. p_n is the partial concentration of the carriers in box n. f_i is the Fermi-Dirac occupation of the state i. Therefore $p_n f_i$ represents the probability that the carrier is located at the state i in box n while the factor $1-p_m f_j$ accounts for the fact that at most one carrier can occupy a single state due to the Pauli exclusion principle. The actual occupation of each state is much smaller than 1 owing to the small carrier density. Here the energy difference $\epsilon_j-\epsilon_i$ in $\gamma_{i,j}$ contains $-eER^x_{n,m}$ when the uniform electric field E is applied in x direction; $R_{n,m}$ is the distance between the box n and m. In equilibrium, the static master equation

$$\sum_m [\Gamma_{n\to m} - \Gamma_{m\to n}] = 0 \tag{6}$$

is satisfied for each box n. The partial concentration p_n can be determined from the master equation under the constraint that $\Sigma_n p_n = pV$, where p is the total carrier concentration (or density) and V is the volume of the system. Therefore the carrier mobility μ is obtained by

$$\mu = \frac{\sum_{n,m} \Gamma_{n\to m} R^x_{n,m}}{pEV}. \tag{7}$$

The dependence of μ on temperature T, electric field E, and the carrier density p is through the macroscopic transition rate.

In the following, we show how the approach can be used to determine the hole mobility in disordered P3HT from first principles. The system consists of $100\times100\times100$ cubes and each cube has a dimension of 1.8 nm, larger than the intersite distance (1.4 nm) estimated from the Gaussian mobility model of P3HT with experimental parameters.[29] Each cube contains 606 atoms, including three P3HT chains with each chain of eight thiophene rings, which leads to a mass density of 1.1 $\mathrm{g/cm^3}$, similar to the experimental value. The top 16 valence bands spreading over 1.4 eV are chosen as the relevant states of the hole carrier. The *ab initio* MD calculations are carried out for a representative box with periodic boundary conditions. The projector augmented wave pseudopotentials[30] and Perdew-Burke-Ernzerhof exchange-correlation functional[31] as implemented in the VASP package[32,33] are used in the calculations. The calculations are performed at Γ point with 300 eV energy cutoff.

The initial structure of the P3HT chains starting from a randomly placed and warped configuration is fully relaxed to reach the local-energy minimum. The *ab initio* Born-Oppenheimer molecular dynamics are performed to bring the system to a desired temperature with repeated velocity scaling. The system is then kept at the desired temperature for 500 fs with 1 fs time step to reach the thermal equilibrium. Finally, the microcanonical production run is carried out for 1000 fs with 1 fs time step for each temperature. To check whether the system is equilibrated within the 1000 fs MD simulations, we calculate the autocorrelation function $C(t)$ of the highest occupied molecular orbital (HOMO) as

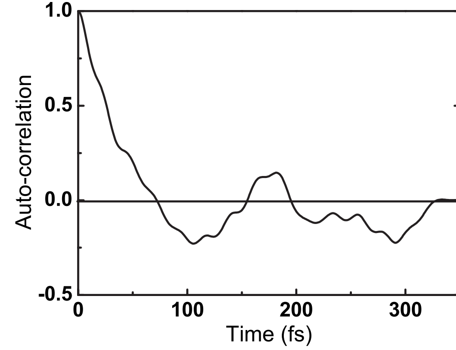

FIG. 3. The time evolution of the autocorrelation function for the HOMO state in the microcanonical MD simulation at $T=300$ K.

$$C(t) = \frac{\langle \epsilon_{\mathrm{HOMO}}(t)\epsilon_{\mathrm{HOMO}}(0)\rangle}{\langle \epsilon^2_{\mathrm{HOMO}}\rangle}, \tag{8}$$

where ϵ_{HOMO} is the energy of HOMO state and the average is taken over 1000 MD steps. The result is shown in Fig. 3 and we find that $C(t)$ decreases by 75% within the first 50 fs, and then has a small oscillation (within 20%) for the remaining time. Therefore we conclude that our simulated system is reasonably equilibrated.

The energies, localized KS orbitals and d_{jk} in Eq. (3) are determined for each MD snapshot during which Eq. (2) is solved by a standard second-order finite-difference method with a time step of 10^{-3} fs. Subsequently, the microscopic transition rate $\gamma_{i,j}$ is obtained via Eq. (4) for both intracube and intercube transitions. This is justified because (i) there is no distinction between intracube and intercube transitions in reality—the carriers simply hop from one localized state to another with no regard to the cubes introduced solely for computational purpose. (ii) The atomic structures in different cubes are randomly chosen and oriented from the different MD snapshots. Therefore we can determine the intercube transition rates based on the relevant intracube transition rates by noting that the transition rates depend most sensitively on the distance between two states. More specifically, the intracube transition rate $\gamma_{i,j}$, where states i and j are located in the same cube, is calculated directly from the *ab initio* molecular dynamics following Eq. (4). On the other hand, the intercube transition rate $\gamma_{i,j}$, where states i and j are located in two neighboring cubes n and m, respectively, is determined from the relevant intracube transition rates shown below. As shown in Fig. 2, states i' and j' are selected from the cube n and m, respectively, so that the distances $R_{ii'}$ and $R_{j'j}$ match as closely as possible to R_{ij}. Since states i' and i (j' and j) fall within the same cube n (m), their intracube transition rate can be calculated by Eq. (4). Finally, the intercube transition rate can be approximated by

$$\langle |c_j^{(i)}(t)|^2/t\rangle = \frac{\langle |c_{i'}^{(i)}(t)|^2/t\rangle + \langle |c_j^{(j')}(t)|^2/t\rangle}{2}. \tag{9}$$

This approach is similar in spirit to the one used by Vukmirovic and Wang.[24] As the last step, the master equation, Eq. (6), is solved iteratively[12] from which the partial concen-

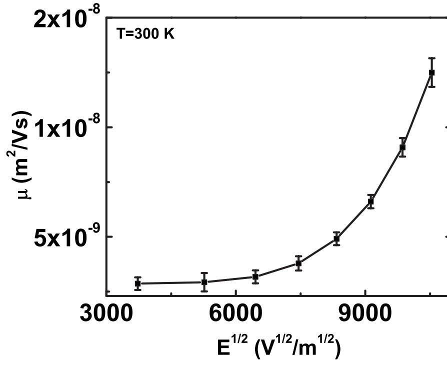

FIG. 4. The variation in carrier mobility due to the structure disorder at $T=300$ K. The solid curve denotes the average value and the error bars represent the standard deviation for ten randomly generated macroscopic structures.

tration p_n can be obtained. Finally the carrier mobility is determined via Eq. (7).

Before discussing the physical aspect of the results, we examine the statistics of the results. To this end, we randomly generate ten different macroscopic structures and calculate their mobility as a function of electric field at 300 K. There are three sources of randomness: (i) the localized wave functions in different cubes are selected randomly from different MD snapshots; (ii) the obtained wave functions are then randomly rotated before placed in the cubes; and (iii) the spatial position of each localized wave function is determined randomly as discussed above. The combination of these randomness gives rise to the different macroscopic structures. We find that the different macroscopic structures yield the mobility values that are within 10% from each other as shown in Fig. 4. Given our modest goal to predict mobility with the correct order of magnitude, the statistics of the results is very encouraging. In particular, the results validate our approach to the intercube transition rates.

We have considered two hole densities 10^{20} and 10^{21} m^{-3} in the simulations, and obtained the similar mobility. This finding is consistent with the experimental observation that the hole mobility is constant for carrier density $<10^{22}$ m^{-3} in P3HT.[29] The hole density of 10^{20} m^{-3} corresponds to an average density of 10^{-6} carrier per cube. In this dilute limit, the motion of a carrier is not influenced by others, therefore the mobility is essentially independent of the hole density. In the following, we will concentrate on the mobility for the hole density of 10^{20} m^{-3}.

We first discuss the mobility as a function of uniform electric field and results are summarized in Fig. 5. It is generally suggested that the field-dependent mobility in many polymers follows approximately Poole-Frenkel form, i.e., $\mu \propto \exp[\gamma(T)\sqrt{E}]$ over an extended range of electric fields.[34–36] Here $\gamma(T)$ is the field activation factor. Examining the logarithm of mobility vs $\sqrt{E}$ from 100 to 350 K, we find that only at 100 K the mobility follows the Poole-Frenkel form over a large range of electric field. At other temperatures, the logarithm of mobility is either constant or a polynomial at low electric fields, and follows a linear relation above a critical field strength of $E=5\times10^7$ V/m. For a P3HT diode with 95 nm thickness (with the similar dimensions to our simulations), it is found experimentally that the hole mobility is constant at the low fields under applied voltages up to 3 V in the temperature range of 255–294 K.[29] This voltage range corresponds to $\sqrt{E}$ in the range of $0-5600$ $\text{V}^{1/2}/\text{m}^{1/2}$, which compares very well to Fig. 5 at 300 K, in which the mobility is constant up to $\sqrt{E}=6000$ $\text{V}^{1/2}/\text{m}^{1/2}$. In addition, it is reported[13] that the logarithm of mobility is approximately constant at low fields and becomes linear above a critical field given by σ/ea; here σ is the Gaussian width of the energy fluctuations due to the static disorder and a is the intersite distance. By using the experimental fitting[29] with $\sigma=98$ meV and $a=1.4$ nm, we arrive at the critical field of 8000 $\text{V}^{1/2}/\text{m}^{1/2}$ for P3HT, which is in good agreement to Fig. 5. Overall, our first-principles simulations reproduce very well the experimental observations.

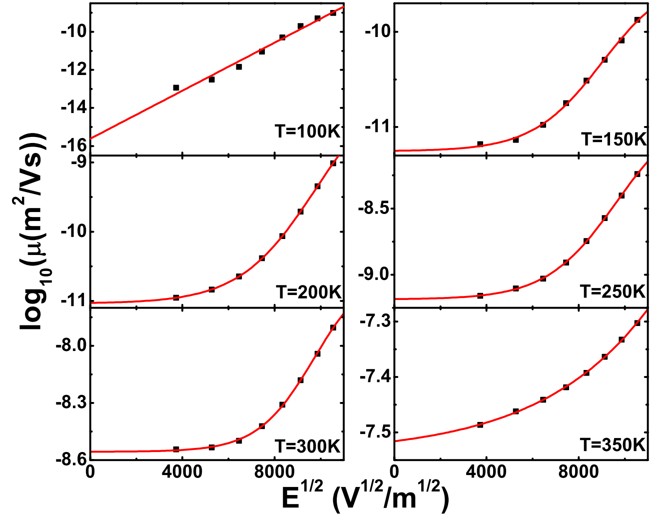

FIG. 5. (Color online) Field dependence of the mobility at various temperatures. Squares: the logarithm of mobility against $E^{1/2}$ at $T=100$, 150, 200, 250, 300, and 350 K. Red curves: fitted curve of the simulated mobility.

The carrier mobility at a vanishing electric field $\mu(E=0,T)$ is given by the extrapolation of the fitted μ vs E curves to $E=0$. Here we compare our simulation results with the experimental data for two types of P3HT: regioregular P3HT (rr-P3HT) and regioirregular P3HT (rir-P3HT). In rr-P3HT all side groups have the same orientation with the head to tail coupling. On the other hand, rir-P3HT has both head to head and tail to tail couplings that could lead to interference of the side groups. In Fig. 6, we show the temperature dependence of the mobility for rr-P3HT and compare against the available experimental values.[37] It has been reported experimentally that the low-field mobility is governed by a universal Arrhenius-type equation: $\mu(E=0,T)=\mu_0\exp(-\Delta/k_BT)$ with the activation energy $\Delta=0.30$ eV; the room-temperature experimental mobility is found to be $\mu_{300\text{ K}}=1.3\times10^{-8}$ $\text{m}^2/\text{V s}$. The corresponding experimental values for rir-P3HT are $\Delta=0.35$ eV and $\mu_{300\text{ K}}=2.8\times10^{-9}$ $\text{m}^2/\text{V s}$.[29] Our first-principles result of $\mu(E=0)$ is 2.9×10^{-9} $\text{m}^2/\text{V s}$ at 300 K, which is in excellent agreement with the experimental result for rir-P3HT, but slightly smaller than the experimental value for rr-P3HT. The

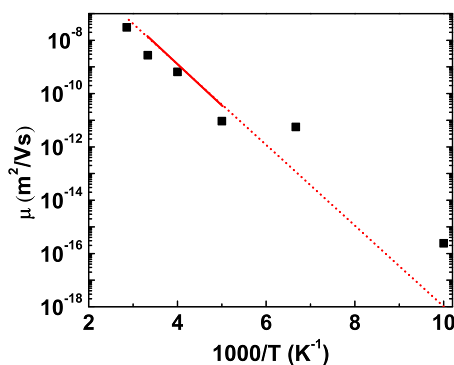

FIG. 6. (Color online) Temperature dependence of the mobility. Squares: simulated low-field mobility $\mu(E=0,T)$ vs inverse temperature. Red line: experimental fit using the Arrhenius relation $\mu(E=0,T)=\mu_0\exp(-\Delta/k_BT)$. The solid line represents the available experimental results from 300 to 200 K; the dotted line gives the full temperature dependence of the Arrhenius equation down to the low temperatures where no experimental result is available.

simulated mobility from 200 to 350 K follows closely the Arrhenius equation as shown in Fig. 6, and the fitted activation energy is 0.31 eV, which compares very well with the experimental value. Finally, we predict that the mobility at low temperatures deviates from the Arrhenius relation, which awaits for experimental verifications.

In the *ab initio* MD simulations, the energy level of each state fluctuates, including the HOMO state which is most relevant to the hole mobility. For a given energy interval, the count that the HOMO state falls between is termed as density of states (DOS) following the nomenclature in this field. In Fig. 7, we present the density of states for $T=100$ K, 200 K, and 300 K, respectively. We find that the density of states follows the Gaussian distribution. At the room temperature (300 K), the fitted Gaussian width is 97 meV, which is in excellent agreement with the experimental value of 98 meV for a P3HT-based hole-only diode.[29] We also find that the Gaussian width becomes larger with increasing temperature because the energy fluctuation is greater.

The Fourier transform for the time dependence of the energy levels is used to identify the relevant phonon modes that

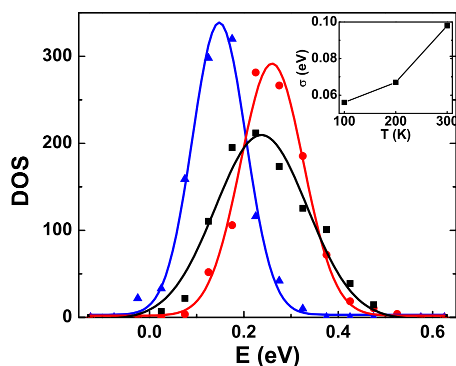

FIG. 7. (Color online) The density of states (counts per energy) at different temperatures. The curves are the Gaussian fits to the computed DOS. Black, red, and blue curves represent $T=300$ K, 200 K, and 100 K, respectively. Inset: the Gaussian width vs temperature.

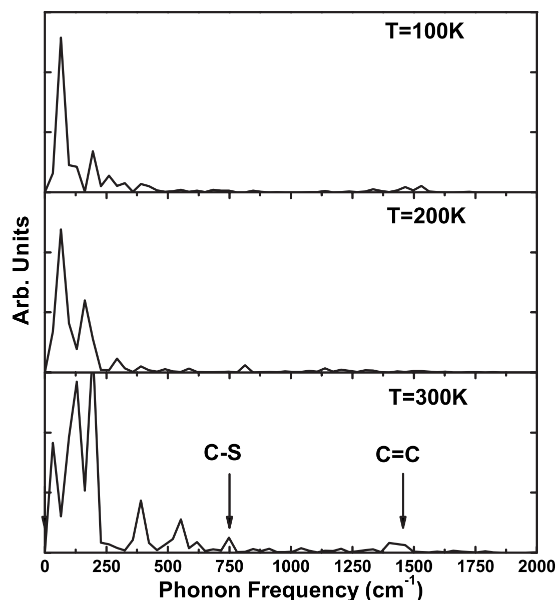

FIG. 8. The Fourier transform of the HOMO energy levels at $T=100$ K, 200 K, and 300 K, respectively. The bottom panel shows the characteristic phonon frequencies corresponding to the stretching modes of C—S and C═C bonds.

contribute to the electron-phonon coupling. Figure 8 shows the Fourier analysis of the time-dependent HOMO energy level. The vibration modes of P3HT are known to have two contributions: one from the bending and torsion modes of the backbones with lower phonon frequencies and the other from the stretching modes with higher frequencies. In particular, the stretching frequency of C—S, C═C, and C—H bonds is 750 cm^{-1}, 1500 cm^{-1}, and 3000 cm^{-1}, respectively. We find that from 100 to 300 K, these lower frequency phonons dominate the hole mobility; beyond 300 K the stretching modes of C—S and C═C bonds become more important. On the other hand, the stretching modes of C—H bonds despite having the highest phonon frequencies do not contribute to the hole mobility. This result is consistent with the finding of Vukmirovic and Wang.[24]

In conclusion, we have proposed a method that can predict carrier mobility in disordered semiconducting polymers and organic semiconductors from first principles. The method is based on the nonadiabatic *ab initio* molecular dynamics and the static master equation without any empirical input or adjustable parameters. We have applied the method to calculate the hole mobility in P3HT conjugated polymers as a function of temperature and electric field and have obtained excellent agreements with the corresponding experimental results. Being general and of predictive power, the method could be used to explore the structure-mobility relation in disordered semiconductors and aid the rational design of these materials.

This work was supported by NSF Solar energy under Grant No. DMR-1035480 and NSF MRI-R^2 under Grant No. DMR-0958596. We acknowledge helpful discussions with Thuc-Quyen Nguyen and Carlos Garcia-Cervera.

[1] J. H. Burroughes, D. D. C. Bradley, A. R. Brown, R. N. Marks, K. Mackay, R. H. Friend, P. L. Burns, and A. B. Holmes, Nature (London) **347**, 539 (1990).
[2] H. Sirringhaus, P. J. Brown, R. H. Friend, M. M. Nielsen, K. Bechgaard, B. M. W. Langeveld-Voss, A. J. H. Spiering, R. A. J. Janssen, E. W. Meijer, P. Herwig, and D. M. de Leeuw, Nature (London) **401**, 685 (1999).
[3] N. S. Sariciftci, D. Braun, C. Zhang, V. I. Srdanov, A. J. Heeger, G. Stucky, and F. Wudl, Appl. Phys. Lett. **62**, 585 (1993).
[4] V. Coropceanu, J. Cornil, D. A. da Silva Filho, Y. Olivier, R. Silbey, and J.-L. Brédas, Chem. Rev. **107**, 926 (2007).
[5] R. W. Munn and R. Silvey, J. Chem. Phys. **83**, 1843 (1985).
[6] K. Hannewald, V. M. Stojanovic, J. M. T. Schellekens, P. A. Bobbert, G. Kresse, and J. Hafner, Phys. Rev. B **69**, 075211 (2004).
[7] V. M. Kenkre, J. D. Andersen, D. H. Dunlap, and C. B. Duke, Phys. Rev. Lett. **62**, 1165 (1989).
[8] A. Miller and E. Abrahams, Phys. Rev. **120**, 745 (1960).
[9] R. A. Marcus, Rev. Mod. Phys. **65**, 599 (1993).
[10] H. Bässler, Phys. Status Solidi B **175**, 15 (1993).
[11] D. Hertel and H. Bässler, ChemPhysChem **9**, 666 (2008).
[12] Z. G. Yu, D. L. Smith, A. Saxena, R. L. Martin, and A. R. Bishop, Phys. Rev. B **63**, 085202 (2001).
[13] W. F. Pasveer, J. Cottaar, C. Tanase, R. Coehoorn, P. A. Bobbert, P. W. M. Blom, D. M. de Leeuw, and M. A. J. Michels, Phys. Rev. Lett. **94**, 206601 (2005).
[14] J. L. Brédas, D. Beljonne, V. Coropceanu, and J. Cornil, Chem. Rev. **104**, 4971 (2004).
[15] G. J. Nan, L. J. Wang, X. D. Yang, Z. G. Shuai, and Y. Zhao, J. Chem. Phys. **130**, 024704 (2009).
[16] J. Kirkpatrick, V. Marcon, J. Nelson, K. Kremer, and D. Andrienko, Phys. Rev. Lett. **98**, 227402 (2007).
[17] S. Athanasopoulos, J. Kirkpatrick, D. Martnez, J. M. Frost, C. M. Foden, A. B. Walker, and J. Nelson, Nano Lett. **7**, 1785 (2007).
[18] W. Q. Deng and W. A. Goddard, J. Phys. Chem. B **108**, 8614 (2004).
[19] J. Nelson, J. J. Kwiatkowski, J. Kirkpatrick, and J. M. Frost, Acc. Chem. Res. **42**, 1768 (2009).
[20] N. G. Martinelli, Y. Olivier, S. Athanasopoulos, M.-C. R. Delgado, K. R. Pigg, D. A. da Silva Filho, R. S. Sánchez-Carrera, E. Venuti, R. G. D. Valle, J.-L. Brédas, D. Beljonne, and J. Cornil, ChemPhysChem **10**, 2265 (2009).
[21] M. Hultell and S. Stafstrom, Chem. Phys. Lett. **428**, 446 (2006).
[22] A. Troisi and G. Orlandi, Phys. Rev. Lett. **96**, 086601 (2006).
[23] A. Troisi, D. L. Cheung, and D. Andrienko, Phys. Rev. Lett. **102**, 116602 (2009).
[24] N. Vukmirović and L. W. Wang, Nano Lett. **9**, 3996 (2009).
[25] N. Vukmirović and L. W. Wang, Phys. Rev. B **81**, 035210 (2010).
[26] W. R. Duncan, W. M. Stier, and O. V. Prezhdo, J. Am. Chem. Soc. **127**, 7941 (2005).
[27] C. F. Craig, W. R. Duncan, and O. V. Prezhdo, Phys. Rev. Lett. **95**, 163001 (2005).
[28] P. V. Parandekar and J. C. Tully, J. Chem. Phys. **122**, 094102 (2005).
[29] C. Tanase, E. J. Meijer, P. W. M. Blom, and D. M. de Leeuw, Phys. Rev. Lett. **91**, 216601 (2003).
[30] P. E. Blöchl, Phys. Rev. B **50**, 17953 (1994).
[31] J. P. Perdew, K. Burke, and M. Ernzerhof, Phys. Rev. Lett. **77**, 3865 (1996).
[32] G. Kresse and J. Hafner, Phys. Rev. B **47**, 558 (1993).
[33] G. Kresse and J. Furthmuller, Phys. Rev. B **54**, 11169 (1996).
[34] A. Abkowitz, H. Bässler, and M. Stolka, Philos. Mag. B **63**, 201 (1991).
[35] P. W. M. Blom, M. J. M. de Jong, and M. G. van Munster, Phys. Rev. B **55**, R656 (1997).
[36] I. H. Campbell, D. L. Smith, C. J. Neef, and J. P. Ferraris, Appl. Phys. Lett. **74**, 2809 (1999).
[37] N. I. Craciun, J. Wildeman, and P. W. M. Blom, Phys. Rev. Lett. **100**, 056601 (2008).